

**Role of Ionic Liquid in Asphaltene Dissolution  
A Combined Experimental and Molecular Dynamics Study**

Vatti, Anoop Kishore; Dey, Poulumi; Acharya, Sriprasad; Kundarapu, Laxman Kumar; Puttapati, Sampath Kumar

**DOI**

[10.1021/acs.energyfuels.2c02076](https://doi.org/10.1021/acs.energyfuels.2c02076)

**Publication date**

2022

**Document Version**

Final published version

**Published in**

Energy and Fuels

**Citation (APA)**

Vatti, A. K., Dey, P., Acharya, S., Kundarapu, L. K., & Puttapati, S. K. (2022). Role of Ionic Liquid in Asphaltene Dissolution: A Combined Experimental and Molecular Dynamics Study. *Energy and Fuels*, 36(16), 9111-9120. <https://doi.org/10.1021/acs.energyfuels.2c02076>

**Important note**

To cite this publication, please use the final published version (if applicable).  
Please check the document version above.

**Copyright**

Other than for strictly personal use, it is not permitted to download, forward or distribute the text or part of it, without the consent of the author(s) and/or copyright holder(s), unless the work is under an open content license such as Creative Commons.

**Takedown policy**

Please contact us and provide details if you believe this document breaches copyrights.  
We will remove access to the work immediately and investigate your claim.

***Green Open Access added to TU Delft Institutional Repository***

***'You share, we take care!' - Taverne project***

**<https://www.openaccess.nl/en/you-share-we-take-care>**

Otherwise as indicated in the copyright section: the publisher is the copyright holder of this work and the author uses the Dutch legislation to make this work public.

# Role of Ionic Liquid in Asphaltene Dissolution: A Combined Experimental and Molecular Dynamics Study

Anoop Kishore Vatti, Poulumi Dey,\* Sriprasada Acharya, Laxman Kumar Kundarapu, and Sampath Kumar Puttapati\*



Cite This: *Energy Fuels* 2022, 36, 9111–9120



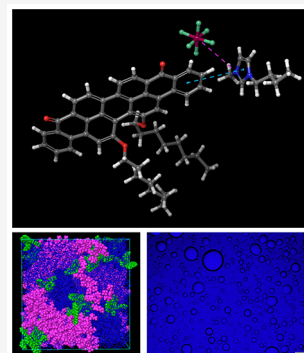
Read Online

ACCESS |

Metrics & More

Article Recommendations

**ABSTRACT:** The role of ionic liquid in asphaltene dissolution is studied using experimental characterization techniques, such as optical microscopic imaging analysis,  $^{13}\text{C}$  nuclear magnetic resonance (NMR), and Fourier transform infrared (FTIR) spectroscopy, along with molecular insights achieved using classical molecular dynamics (MD) simulations. The dissolution behavior of the asphaltenes in 1-butyl-3-methylimidazolium hexafluorophosphate ( $[\text{BMIM}][\text{PF}_6]$ ) ionic liquid along with organic solvents, i.e., toluene and hexane, is investigated using optical images. The behavior of asphaltene aggregates in the solvent plus ionic liquid mixture is probed using FTIR and  $^{13}\text{C}$  NMR spectroscopic techniques. The structural and dynamical properties of the asphaltene aggregates mainly end-to-end distance, the diffusion coefficient of the asphaltene molecules, and the trajectory density contour of the asphaltene in the solvent plus ionic liquid mixture are probed using MD simulations. It is concluded from our combined experimental–MD study that the ionic liquid plays a key role in asphaltene separation from organic solvents under study.



## INTRODUCTION

Heavy crude oil mainly consists of four classes, i.e., saturates, aromatics, resins, and asphaltenes, referred to as SARA. The heaviest component out of these four classes is asphaltenes. Understanding the asphaltene behavior is key for efficient recovery of the heavy crude oil from the conventional hydrocarbon reservoirs. In recent times, there has been a drastic increase in the production of the heavy crude oil. Asphaltenes, which are a major constituent of the heavy crude oil, are responsible for operational problems, such as sludge formation in the bottom of the crude oil storage tanks, coke formation, deactivation of refinery catalysts, etc.<sup>1–4</sup> Further, asphaltenes reduce petroleum productivity near the wellbore region by increasing the skin factor, and also, the fluidity of the heavy oil in pipelines is affected as a result of the highly viscous nature of the asphaltenes.<sup>5–7</sup> As a result of the non-biodegradable nature of asphaltenes, their release into the aquatic bodies has a severe adverse impact on marine life.

Asphaltenes mainly consist of polyaromatic hydrocarbons, alkyl-type side chains, and polar heteroatoms, such as oxygen, sulfur, nitrogen, etc.<sup>8</sup> In the heavy crude oil, the asphaltene component holds the major fraction.<sup>9</sup> Asphaltenes form aggregates in *n*-alkanes, water,<sup>10</sup> and water–oil emulsion<sup>11</sup> and are responsible for the high viscosity of crude oil.<sup>4,12</sup> The chemical treatment of asphaltenes is done using cyclic aromatic compounds, such as benzene, toluene, xylene, and pyridine, in which asphaltene is soluble. These solvents are, however, hazardous and volatile. On the other hand, asphaltenes are insoluble in *n*-alkanes, e.g., pentane, heptane, and hexane.<sup>13</sup>

The handling of asphaltene aggregates in the up- or downstream petroleum sector needs alternate solvents that have excellent thermal and chemical stability and are inflammable, non-hazardous, and non-toxic. In this regard, ionic liquids (ILs) are investigated, which played a key role in delivering smart solutions<sup>14</sup> and exhibit excellent asphaltene aggregation inhibition properties.<sup>15–18</sup>

ILs are compounds that entirely consist of ions and have a melting point below 100 °C.<sup>19</sup> ILs can become involved in various interactions ranging from weak, non-isotropic forces to strong Coulomb interactions. They have free ions, which make them electrically conductive in nature. They are usually chemically stable in nature, have a very low vapor pressure, and are non-flammable. ILs have received enormous attention lately to recover bitumen from oil sands<sup>20,21</sup> and as an enhanced oil recovery solvent.<sup>22</sup> Boukherissa et al.<sup>23</sup> investigated the mechanism of new types of IL salts, such as 1-propylboronic acid-3-alkylimidazolium bromides and 1-propenyl-3-alkylimidazolium bromides. The boronic acid moiety in the chain of IL bonds with asphaltene and drastically reduces the size of the asphaltene aggregates. Ogunlaja et al.<sup>24</sup> synthesized three ILs, mainly 1-butyl-3-methylimidazolium

Received: June 23, 2022

Revised: July 30, 2022

Published: August 10, 2022



chloride, 1-butyl-3-methylimidazolium nitrate, and 1-methyl-1*H*-imidazole-3-ium-2-carboxybenzoate, to disperse the asphaltenes. It is observed that the  $\pi$ - $\pi$  interactions dominate between the IL cation and asphaltene. Further, density functional theory (DFT) calculation-based interaction energies revealed that 1-butyl-3-methylimidazolium chloride is more reactive than the other synthesized ILs. Sakthivel et al.<sup>25</sup> conducted experimental studies using ultraviolet–visible (UV–vis), Fourier transform infrared (FTIR), and <sup>13</sup>C nuclear magnetic resonance (NMR) spectroscopy to study the dissolution of tank bottom sludge containing mainly asphaltene components. The dissolution was probed in the presence of nine synthesized ILs. It was observed that 1-butyl-3-methylimidazolium hexafluorophosphate ([BMIM][PF<sub>6</sub>]) IL performs better in both toluene and hexane solvents in comparison to other ILs. Sakthivel et al.<sup>26</sup> also investigated the heavy crude oil dissolution in the aliphatic ILs along with toluene, heptane, hexane, decane, and ethyl acetate solvents using UV–vis, FTIR, and <sup>13</sup>C NMR spectroscopy. It was observed that 10% IL is sufficient for complete dissolution of the heavy crude oil in organic solvent. Further, [Et<sub>3</sub>NH][H<sub>2</sub>PO<sub>4</sub>] IL showed superior performance with regard to dissolving heavy crude oil in toluene than [Et<sub>3</sub>NH][CH<sub>3</sub>COO].

Subramanian et al.<sup>27</sup> worked on the reduction of the viscosity of Mexican heavy oils/Canadian and Venezuelan bitumen extra-heavy oil using the ILs. The inhibition of the asphaltene aggregation is observed using 1-butyl-3-methylimidazolium cation-based ILs along with anions, such as chloride, thiocyanate, and tetrafluoroborate. The results showed that acid–base, charge-transfer interface, and molecular interactions between the ILs and the asphaltene molecules play a vital role in viscosity reduction and disaggregation of asphaltene. Hernandez-Bravo et al.<sup>28</sup> performed experiments, DFT calculations, and molecular dynamics (MD) simulations to investigate the interaction of different ILs with asphaltene. It was observed that the interactions between the IL cation and asphaltene  $\pi$  were dominant. C<sub>23</sub>H<sub>36</sub>BrN IL was more effective in reducing the viscosity of the heavy crude oil in comparison to the C<sub>18</sub>H<sub>35</sub>BrN<sub>2</sub>, C<sub>19</sub>H<sub>34</sub>BrN, C<sub>23</sub>H<sub>42</sub>Br<sub>2</sub>N<sub>4</sub>, C<sub>23</sub>H<sub>39</sub>BrN<sub>2</sub>, and C<sub>17</sub>H<sub>38</sub>BrN ILs. Martinez-Mora et al.<sup>29</sup> performed experimental and theoretical analysis of heavy crude oil rheological properties in the presence of imidazolium-based ILs. Their results showed that the considered 24 ILs reduced the viscosity of the heavy crude oil, where ILs [C<sub>6</sub>bim][PF<sub>6</sub>], [phetbim][PF<sub>6</sub>], and [C<sub>9</sub>bim][NTf<sub>2</sub>] were the most effective in reducing the viscosity in comparison to other considered ILs.

The above-mentioned existing work highlights the importance of ILs in asphaltene dissolution in crude oil samples. However, it is worthwhile to note that the crude oil assay contains numerous compounds, including asphaltene. It is, thus, required to go beyond the state-of-the-art studies to perform a rational selection of IL for asphaltene separation purely dependent upon the asphaltene–IL interaction. Within this work, we perform a thorough investigation of the IL interaction with pure asphaltene. Such a kind of study is lacking in the existing literature to the best of our knowledge. We have used experimental techniques and MD simulations to achieve deep insights into pure asphaltene dissolution in the presence of IL. Within experiments, the optical images, <sup>13</sup>C NMR and FTIR spectroscopy results are analyzed in depth to understand the effect of the IL on the asphaltene dissolution.

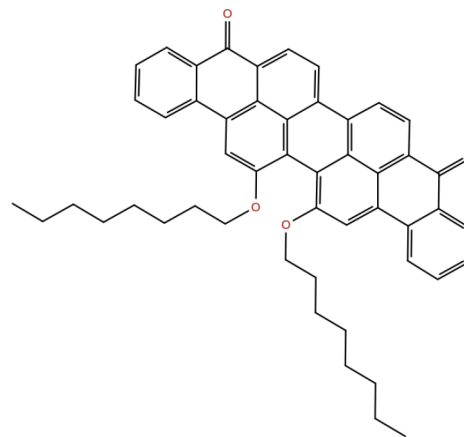
We have adopted a novel approach of end-to-end analysis to quantify the asphaltene aggregation behavior. We report relevant structural and dynamical properties based on MD simulations, viz., end-to-end distance, diffusion coefficient, and trajectory density contours, of asphaltene molecules in the presence of IL and in organic solvents, i.e., toluene and hexane.

## EXPERIMENTAL DETAILS

We have used 95% pure asphaltene (Violanthrone-79)(C<sub>50</sub>H<sub>48</sub>O<sub>4</sub>). The sample is procured from BLD Pharmatech, Limited. Toluene and *n*-hexane are used as organic solvents. 1-Butyl-3-methylimidazolium hexafluorophosphate ([BMIM][PF<sub>6</sub>]) IL with  $\geq 97\%$  high-performance liquid chromatography (HPLC) purity procured from Sigma-Aldrich is used. The IL in asphaltene–toluene/hexane samples is probed using two primary methods, viz., filter paper<sup>30</sup> and the microscopic method.<sup>31,32</sup> The methodology adopted for the sample preparation and the filter paper method is described in detail in our recent work.<sup>33</sup> The samples are prepared and transferred in a Petri dish. During optical imaging, Petri dishes are closed with the lid to avoid the evaporation of the organic solvents. An Olympus IX73 inverted microscope is used to capture the images. A FT/IR-6300 (Jasco) is used for FTIR, and the samples are scanned with a scanning resolution of 0.07 cm<sup>-1</sup> and in the wavenumber range of 400–4000 cm<sup>-1</sup>. A Bruker AV-400 NMR spectrometer is used for the <sup>13</sup>C NMR characterization.

## COMPUTATIONAL DETAILS

The probable molecular mass of the asphaltene is approximately 750 g/mol.<sup>34</sup> Moreover, the range of the molecular mass of asphaltene compounds is between 500 and 1000 g/mol.<sup>35</sup> The asphaltene (C<sub>50</sub>H<sub>48</sub>O<sub>4</sub>) Violanthrone-79 compound has a molecular weight of 712.9 g/mol. Thus, the proximity of the molecular weight of this compound to 750 g/mol motivated us to choose it as a model compound to explore its aggregation behavior using MD simulations. Asphaltene molecules contain aromatic rings, a linear aliphatic side chain, and oxygen heteroatoms in the polyaromatic core, as shown in Figure 1. In addition, toluene, hexane, and 1-butyl-3-methylimidazo-

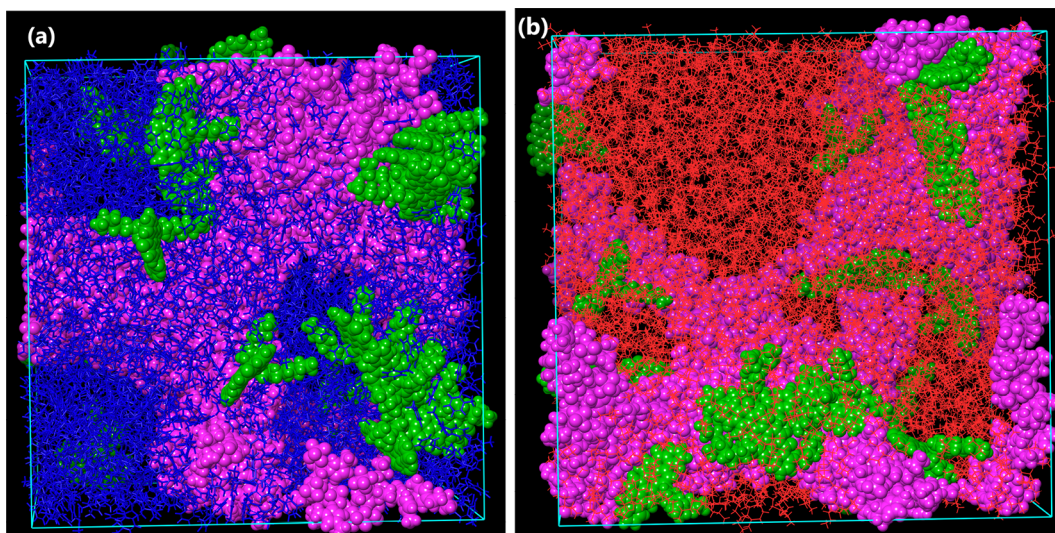
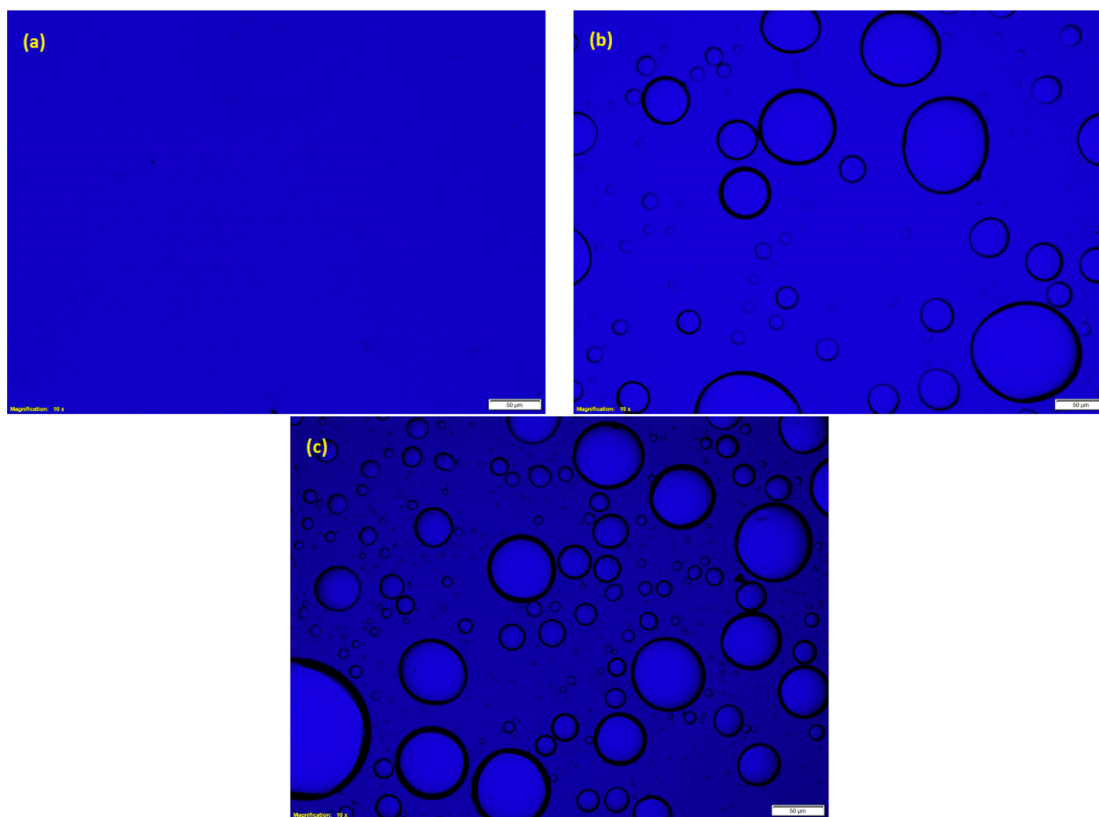


**Figure 1.** Asphaltene (Violanthrone-79) two-dimensional (2D) molecular structure.

lium hexafluorophosphate ([BMIM][PF<sub>6</sub>]) IL explicit molecules are considered. Four different mixtures are considered, as shown in Table 1. The bonded and Lennard-Jones interactions in the modeled systems are described using the latest optimized parameters for liquid simulations (OPLS4)<sup>36</sup> force fields. To perform MD simulations, we used Desmond<sup>37</sup> MD code within the Schrödinger simulation software.<sup>38</sup> The time step of 2 fs is used to integrate equations of motion. A Martyna–Tobias–Klein barostat with a relaxation time of 2 ps with isotropic coupling and a Nosé–Hoover thermostat with a relaxation time of 1 ps are used. The cutoff considered for non-

**Table 1. Number of Asphaltene, Toluene, Hexane, and [BMIM][PF<sub>6</sub>] IL Molecules along with the Simulation Box Sizes for Considered Mixtures**

mixture	asphaltene molecules	toluene molecules	hexane molecules	[BMIM][PF <sub>6</sub> ] IL	simulation box size (Å <sup>3</sup> )
asp + toluene	24	2976			81.04 × 82.65 × 81.77
asp + [BMIM][PF <sub>6</sub> ] + toluene	24	2668		308	83.25 × 83.31 × 85.36
asp + hexane	24		2976		90.62 × 87.18 × 86.91
asp + [BMIM][PF <sub>6</sub> ] + hexane	24		2684	292	90.15 × 89.49 × 88.33

**Figure 2.** Snapshots of the MD NVT run for (a) asphaltene + toluene + [BMIM][PF<sub>6</sub>] at 77.71 ns and (b) asphaltene + hexane + [BMIM][PF<sub>6</sub>] IL at 66.14 ns are shown for 24 asphaltene molecules. The color coding is as follows: asphaltene is green; [BMIM][PF<sub>6</sub>] IL is pink; toluene is blue; and hexane is red.**Figure 3.** Optical microscopic images of (a) fully dissolved asphaltene in toluene, (b) asphaltene in toluene along with 0.02 mL of [BMIM][PF<sub>6</sub>] IL, and (c) asphaltene in toluene along with 0.04 mL of [BMIM][PF<sub>6</sub>] IL. The length scale of each optical image is 50 μm.



**Figure 4.** Optical microscopic images of (a) asphaltene in hexane and (b) asphaltene in hexane along with 0.01 mL of [BMIM][PF<sub>6</sub>] IL. The length scale of each optical image is 50  $\mu\text{m}$ .

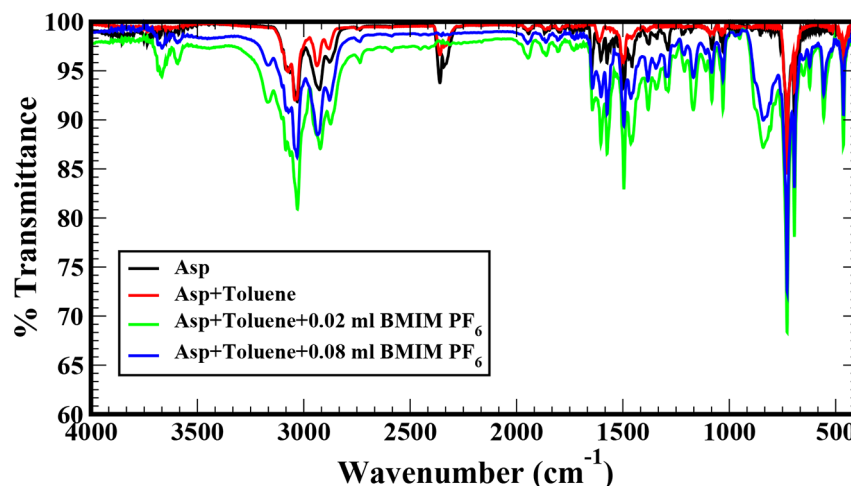


**Figure 5.** FTIR spectra of the considered samples are shown. The black line depicts the spectrum of the pure asphaltene sample. The red line shows the spectrum of completely dissolved asphaltene in toluene; the green line is for the asphaltene–toluene mixture after the addition of 0.02 mL of [BMIM][PF<sub>6</sub>] IL; and the blue line denotes the asphaltene–toluene mixture with 0.08 mL of [BMIM][PF<sub>6</sub>] IL.

bonded interactions is 9 Å. The *NPT* equilibration run of 20 ns and the *NVT* production run of 80 ns are performed. The MD snapshot of the asphaltene + [BMIM][PF<sub>6</sub>] IL in toluene at 77.71 ns is shown in Figure 2a, and the MD snapshot of the asphaltene + [BMIM][PF<sub>6</sub>] IL in hexane at 66.14 ns is shown in Figure 2b. The snapshots clearly show the asphaltene molecules aggregates as depicted by the green color in the presence of the IL (shown in pink) in both toluene and hexane solvents.

## RESULTS AND DISCUSSION

**Optical Microscopy.** To understand the role of IL in separating asphaltenes from the toluene/hexane solvent, we have used the optical microscopy technique to investigate how the IL disintegrates and separates asphaltene from organic solvents, mainly toluene (where asphaltene is soluble) and hexane (where asphaltene is insoluble). Figure 3a shows the optical microscope image of asphaltene in toluene, where no aggregates are visible. Later, 0.02 mL of [BMIM][PF<sub>6</sub>] IL is added in small increments. The spontaneous emulsification is observed as shown in Figure 3b as a result of the presence of the [BMIM][PF<sub>6</sub>] IL. Figure 3c shows the result for the highest amount of the IL, i.e., 0.04 mL, in the asphaltene–toluene mixture. Our study revealed that the presence of IL in the asphaltene–toluene mixture induces spontaneous emulsification, where the IL droplets are stabilized by the asphaltenes

appearing at the droplet boundary in the case of the toluene solvent.

Figure 4a shows the optical microscope image of asphaltene in hexane, and Figure 4b shows the optical microscope image of 0.01 mL of [BMIM][PF<sub>6</sub>] IL in the asphaltene–hexane mixture. It is evident from the images that a clear separation of the asphaltene particles happens with the addition of a small quantity of 0.01 mL of the IL in the asphaltene–hexane sample. Several droplets are formed, and the IL holds the asphaltene particles as a result of the strong interaction between IL–asphaltene than the asphaltene–hexane pair. Hence, an interesting conclusion that a small amount of IL is sufficient for the efficient separation of asphaltene particles from the hexane solvent can be drawn from this study. Further, the [BMIM][PF<sub>6</sub>] IL is thermally stable up to 610 K. Therefore, the regeneration of the IL is possible using thermal distillation.<sup>39</sup>

**FTIR and <sup>13</sup>C NMR.** Figure 5 shows the change in percent transmittance as a function of the wavenumber for different FTIR samples considered in this work. The absorption modes seen around 1450 cm<sup>-1</sup> correspond to the C–H bending frequency; the peak at 2935 cm<sup>-1</sup> corresponds to the C–H stretching frequency; the peak at 3030 cm<sup>-1</sup> corresponds to the aromatic C–H stretch; and the peak at 1490–1606 cm<sup>-1</sup> corresponds to the conjugated C=C. The difference in the

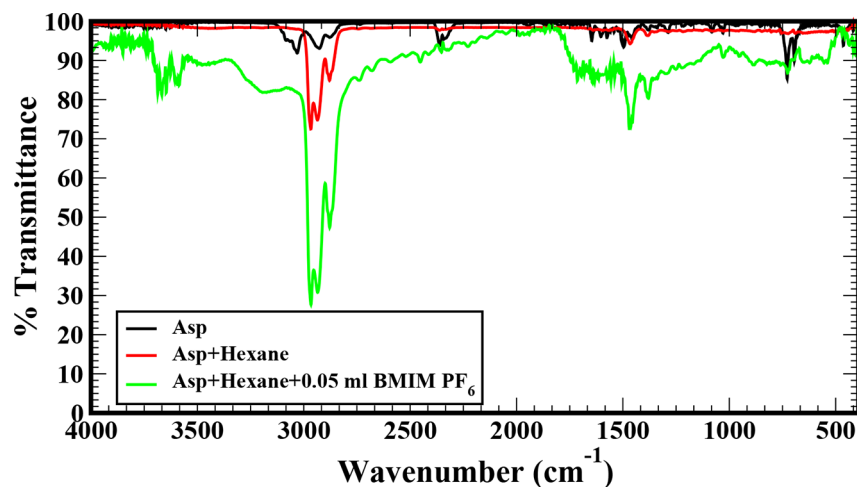


**Figure 6.** FTIR spectra of the considered samples are shown. The black line depicts the spectrum of the pure asphaltene sample. The red line shows the spectrum of asphaltene in hexane, and the green line is for the asphaltene–hexane mixture after the addition of 0.05 mL of [BMIM][PF<sub>6</sub>] IL.

peak intensities can be associated with the amount of asphaltene aggregates present in the sample.<sup>33</sup> The red line depicts the infrared (IR) spectrum of an asphaltene–toluene mixture, whereas the black line depicts the IR spectrum of pure asphaltene. The peak intensities denoted by the red line are slightly lower than those of pure asphaltene, where asphaltene is fully dissolved in toluene and there are no visible aggregates present in the sample. The green line, which depicts the IR spectrum of the sample containing the asphaltene, toluene, and 0.02 mL of [BMIM][PF<sub>6</sub>] IL mixture, has the highest peak intensities compared to the other samples, indicating the presence of asphaltene separated from the toluene solvent because of the IL. The percent transmittance value decreasing as the number of aggregates in the sample increases is also observed in our earlier work.<sup>33</sup> It can also be seen in Figure 5 that, with a further increase in the concentration to 0.08 mL of [BMIM][PF<sub>6</sub>], the peak intensity decreases moderately, as denoted by the blue line. We can conclude from Figure 5 that, as the concentration of [BMIM][PF<sub>6</sub>] increases, the asphaltene separation increases as a result of the formation of the numerous IL droplets, where asphaltene is separated, leading to the smaller size of the aggregates. There is an increase in peak intensity when 0.02 mL of the IL is added to the asphaltene dissolved in toluene mixture as a result of the formation of the aggregates. On the other hand, when 0.04 mL of the IL is added, smaller aggregates are observed as visible in the optical images (Figure 3).

Figure 6 shows the FTIR spectra for the samples treated with the hexane solvent. The FTIR spectrum of pure asphaltene has the highest percent transmittance value, as shown by the black line. There is a significant reduction in the percent transmittance value in the FTIR spectrum of the asphaltene–hexane mixture (indicated by the red line) in comparison to the pure asphaltene spectrum. This aligns with the fact that asphaltene is insoluble in hexane and aggregates are present in the hexane solvent. Further, when the sample is treated with [BMIM][PF<sub>6</sub>] IL, the later quickly starts to isolate asphaltene particles from hexane, leading to the formation of numerous aggregates. As a result of this, the percent transmittance value is the least for asphaltene + hexane + [BMIM][PF<sub>6</sub>] IL, as indicated by the green line. Hence, it can be concluded that [BMIM][PF<sub>6</sub>] has higher affinity to separate

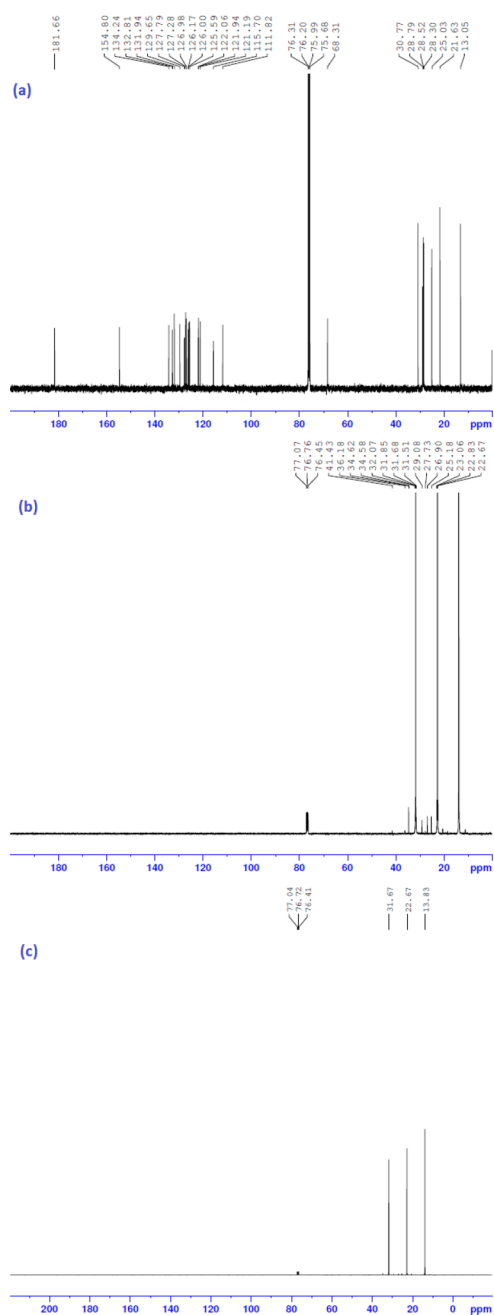
asphaltene particles in hexane in comparison to the toluene solvent, which is supported by our optical image results.

Figure 7 shows the <sup>13</sup>C NMR spectra of the (a) pure asphaltene, (b) asphaltene–hexane mixture, and (c) asphaltene–hexane along with 0.05 mL of [BMIM][PF<sub>6</sub>] IL. Numerous peaks are observed in Figure 7a in the region of 10–30 ppm clearly indicating the CH<sub>2</sub> and CH<sub>3</sub> peaks of asphaltene; 120–160 ppm shows the aromatics; and the peak around 180 ppm is the indication of the >C=O group present in asphaltene. It is interesting to note that, with the addition of the hexane solvent, peaks between 10 and 30 ppm become more pronounced (Figure 7b), and a few peaks disappear between 10 and 30 ppm when IL is added, as seen in Figure 7c. The aromatic peaks disappear when hexane and IL are added to the asphaltene sample, which clearly indicates the strong interaction of asphaltene with IL. It is interesting to note that the aromatic peaks disappeared slightly for the asphaltene–toluene–[BMIM][PF<sub>6</sub>] IL solvent in comparison to the <sup>13</sup>C NMR spectra of the pure asphaltene sample, whereas the peaks disappeared completely for hexane. Our conclusion is supported by the earlier work, where aromatic peaks were observed to disappear after adding [Et<sub>3</sub>NH][CH<sub>3</sub>COO] IL in the mixture of heptane and crude oil containing asphaltene.<sup>26</sup>

**End-to-End Distance.** We have calculated the end-to-end distance of the asphaltene molecules in the presence and absence of IL. The distance between the end of the alkyl side chain to the other end is termed as the end-to-end distance. It is a crucial quantity to analyze the size of the aggregates as a result of the fact that the alkyl side chains are flexible on the longer length scales and stiff on shorter length scales in the asphaltene aggregation process. In our earlier works, the end-to-end distance of asphaltene is calculated in an aqueous environment using various water models<sup>10</sup> and in organic solvents as well.<sup>33</sup> The distance is evaluated using a worm-like chain model<sup>40</sup> considering the semi-flexible side chains.<sup>41</sup> The molecule-averaged end-to-end distance over the entire production MD run trajectory is calculated using the following equation:<sup>41</sup>

$$\langle R_E^2 \rangle = 2l_p L_0 [1 - (l_p/L_0)(1 - \exp(-L_0/l_p))] \quad (1)$$

where the mean squared end-to-end distance is denoted as  $\langle R_E^2 \rangle$ , the persistence length is  $l_p$ , and the extended chain length is denoted as  $L_0$ .



**Figure 7.**  $^{13}\text{C}$  NMR spectra for the samples: (a) pure asphaltene in  $\text{CDCl}_3$ , (b) asphaltene + hexane, and (c) asphaltene + hexane + 0.05 mL  $[\text{BMIM}][\text{PF}_6]$ .

Figure 8 shows the end-to-end distance versus time for asphaltene molecules in (a) pure toluene, (b) the toluene and  $[\text{BMIM}][\text{PF}_6]$  mixture, (c) pure hexane, and (d) the hexane and  $[\text{BMIM}][\text{PF}_6]$  mixture. The end-to-end distance, persistence length, extended chain length, time series standard deviation, and molecular distribution standard deviation are summarized in Table 2. The calculated end-to-end distances of asphaltene molecules are 11.84 Å in pure toluene and 11.21 Å in pure hexane. The slightly lower value in hexane is in accordance with the strong aggregation behavior of asphaltene in hexane, in which it is insoluble. The lower end-to-end distance value indicates a smaller distance between alkyl side chains, indicating that aggregates are stable. When we add  $[\text{BMIM}][\text{PF}_6]$  IL, there is a slight decrease in the end-to-end

distance in the case of the toluene–asphaltene mixture, i.e., 11.66 Å, and a slight increase in the case of the hexane–asphaltene mixture, i.e., 11.56 Å, in comparison to asphaltene in pure solvents, i.e., toluene/hexane. It is interesting to note that, for the asphaltene–hexane–IL mixture, asphaltene dissolution is higher as a result of which a slight increase in the end-to-end distance is observed. The alkyl side chain can adapt based on the solvent in which asphaltenes are present. As a result of this, there is slight difference in the values of the end-to-end distance for considered pure organic solvents and for the organic solvents with IL. Overall, a lower end-to-end distance is observed in the case of asphaltene in the hexane solvent than in toluene in the absence or presence of IL, depicting the stability of aggregates as a result of the insoluble nature of asphaltene in hexane. The extended chain length is found to be approximately 24 Å for all four mixtures. The molecular distribution standard deviation is found to be approximately 4 Å, which shows that the change in the end-to-end distance within asphaltene molecules is uniform, irrespective of the concentration. The persistence length specifies the length beyond which there are no correlations; i.e., the alkyl side chains are stiffer for distances larger than the persistence length. Interestingly, the persistence length is found to be different for all four different cases studied. We have observed in our simulations that there is a  $\pi$ – $\pi$  stacking present between the aromatic part of the asphaltene and aromatic IL.

**Diffusion Coefficient.** The asphaltene molecule diffusion coefficient is calculated using the following equation:<sup>42</sup>

$$D = \frac{1}{6} \lim_{t \rightarrow \infty} \frac{d}{dt} \langle |\vec{x}(t) - \vec{x}(0)|^2 \rangle \quad (2)$$

where mean-square displacement is denoted as  $\langle |\vec{x}(t) - \vec{x}(0)|^2 \rangle$  and angled brackets indicate an ensemble average. The calculated diffusion coefficients of asphaltene are shown in Table 3 for different solvent mixtures considered within this work. It is evident that the diffusion coefficient of asphaltene is higher in hexane in comparison to toluene as a result of the formation of the aggregates in hexane. It is interesting to note that, with the addition of the IL to pure hexane, we noticed a reduction in the diffusion coefficient in comparison to pure hexane. This indicates that the mobility of asphaltene is drastically reduced in the presence of IL. Similarly, we noticed a decrease in the diffusion coefficient of asphaltene for the toluene solvent as well in the presence of IL. Overall, we observed the trend that the IL lowers the mobility of asphaltene for both of the solvents under consideration.

**Density Contours.** The asphaltene aggregate cross-section contours are calculated by taking layers of a specified thickness perpendicular to the chosen geometrical coordinate axis to calculate the cross-sectional density. To calculate the density, the van der Waals volume fraction of each atom that overlaps the layer is multiplied by their atomic mass, and the result is summed over all specified atoms and then divided by the volume of the layer. Further, to calculate the cross-sectional density contours, the layer is divided into cubes, and the volume fraction of each atom that overlaps each cube is evaluated, weighted by the atomic mass, summed, and divided by the cube volume to provide the density in the cube.

The asphaltene trajectory density contours for the considered asphaltene + solvent + IL mixture are shown in Figure 9. Figure 9a illustrates the asphaltene trajectory density contour for asphaltene in the pure toluene solvent; Figure 9b

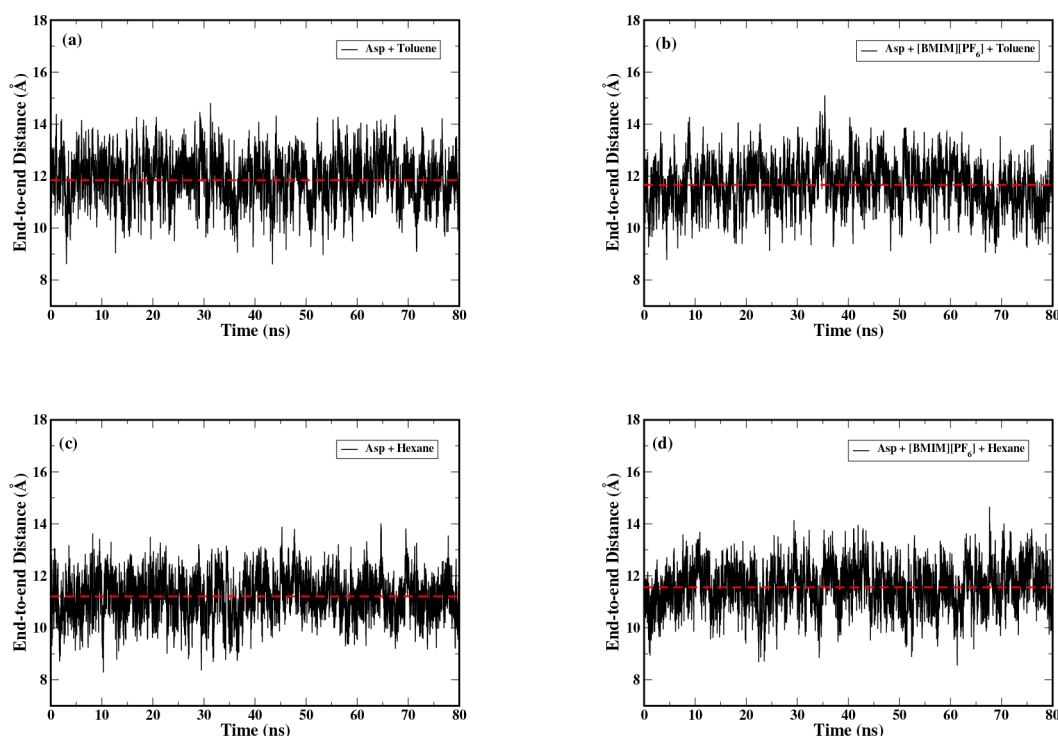


**Figure 8.** Calculated end-to-end distance versus time are shown for (a) asphaltene molecules in pure toluene, (b) asphaltene molecules in the toluene and [BMIM][PF<sub>6</sub>] mixture, (c) asphaltene molecules in pure hexane, and (d) asphaltene molecules in the hexane and [BMIM][PF<sub>6</sub>] mixture. The averaged end-to-end distance is indicated by a red dashed line in each of the sub-figures.

**Table 2.** Calculated End-to-End Distance of Asphaltene Molecules, Extended Chain Length, Persistence Length, Time Series Standard Deviation ( $\sigma$ ) Related to the End-to-End Distance, and Molecular Distribution Standard Deviation Values Shown for Different Asphaltene + Solvent + IL Mixtures over 80 ns of Production Run

mixture	end-to-end distance (Å)	persistence length (Å)	extended chain length (Å)	time series, $\sigma$ (Å)	molecular distribution standard deviation (Å)
asp + toluene	11.84	3.76	24.65	0.84	4.13
asp + [BMIM][PF <sub>6</sub> ] + toluene	11.66	3.67	24.46	0.84	4.10
asp + hexane	11.21	3.36	24.47	0.76	4.02
asp + [BMIM][PF <sub>6</sub> ] + hexane	11.56	3.57	24.52	0.79	4.01

**Table 3.** Calculated Diffusion Coefficients Shown for Four Different Asphaltene Mixtures along with the Time Series Standard Deviation

mixture	diffusion coefficient (m <sup>2</sup> /s)	standard deviation, $\sigma$ (Å)
asp + toluene	$3.23 \times 10^{-10}$	$3.65 \times 10^{-13}$
asp + [BMIM][PF <sub>6</sub> ] + toluene	$1.09 \times 10^{-10}$	$0.67 \times 10^{-13}$
asp + hexane	$3.73 \times 10^{-10}$	$5.36 \times 10^{-13}$
asp + [BMIM][PF <sub>6</sub> ] + hexane	$0.062 \times 10^{-10}$	$0.0092 \times 10^{-13}$

illustrates the asphaltene trajectory density contour for asphaltene in toluene + [BMIM][PF<sub>6</sub>]; Figure 9c shows the asphaltene trajectory density contour for asphaltene in the pure hexane solvent; and Figure 9d shows the density contour for asphaltene in hexane + [BMIM][PF<sub>6</sub>]. It is evident from the density contour shown in Figure 9a that the density of asphaltene molecules is spread across the cubic box because of the soluble nature of asphaltene in toluene. On the other hand, a clear aggregation of asphaltene is visible in Figure 9c. With the addition of [BMIM][PF<sub>6</sub>] IL in the asphaltene–toluene mixture, we observed the formation of delocalized asphaltene aggregates, as seen in Figure 9b. Further, when [BMIM][PF<sub>6</sub>] IL is added to the asphaltene–hexane mixture, we could notice

that the large aggregate cluster is broken into several numerous aggregates as a result of the IL cation and asphaltene  $\pi$  interactions (Figure 9d).

## CONCLUSION

In this work, we investigated the dissolution of asphaltene in toluene/hexane in the absence and presence of the [BMIM]-[PF<sub>6</sub>] IL using experimental techniques, such as optical microscopy, FTIR, and <sup>13</sup>C NMR, and using MD simulations. The optical microscopy images clearly show distinct separation of asphaltene in hexane when [BMIM][PF<sub>6</sub>] IL is added, and to a great extent asphaltene particles can also be separated from toluene by the addition of IL. The FTIR spectra intensity increases in the presence of the aggregates in the IL + solvent mixture and later decreases for the toluene solvent as a result of spontaneous emulsification when a higher amount of IL is added. Aromatic peaks in <sup>13</sup>C NMR disappear when the IL is added to the asphaltene–hexane mixture, indicating stronger interaction between asphaltene and [BMIM][PF<sub>6</sub>] IL. The slightly low value of the end-to-end distance of asphaltene observed for hexane indicates that the aggregates are stable. The diffusion coefficient of the asphaltene is lower in the hexane + IL mixture in comparison to the toluene + IL mixture

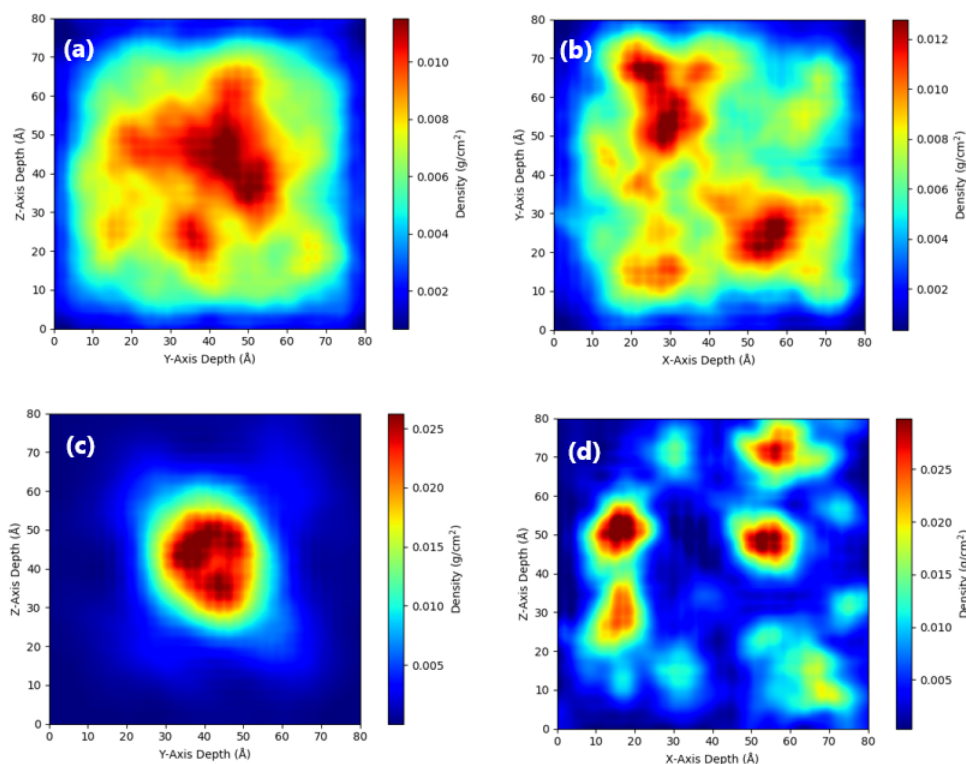


**Figure 9.** Trajectory density contours for (a) asphaltene in pure toluene, (b) asphaltene in toluene + [BMIM][PF<sub>6</sub>] IL, (c) asphaltene in pure hexane, and (d) asphaltene in hexane + [BMIM][PF<sub>6</sub>] IL. The dark red color denotes the maximum trajectory density (g/cm<sup>3</sup>), whereas the dark blue color denotes the minimum trajectory density (g/cm<sup>3</sup>).

as a result of maximum separation of asphaltene from the hexane solvent. The trajectory density contour shows that several numerous asphaltene aggregates are formed in the presence of the IL in the hexane solvent, clearly exhibiting the enhanced asphaltene separation. Therefore, we conclude that IL can disengage the large aggregates to several small aggregates in the hexane solvent. Both the experiments and MD simulations suggest that a minimal quantity of the IL is sufficient to separate asphaltene from hexane and toluene. The performance of IL is superior in hexane in comparison to toluene for asphaltene particle separation. Further, the screening of IL for asphaltene separation also depends upon various other physical and chemical properties of IL, such as viscosity, thermal stability, and chemical affinity, and also, recovery of the IL must be taken into account; therefore, IL selection has to be performed meticulously.

## AUTHOR INFORMATION

### Corresponding Authors

**Poulumi Dey** – Department of Materials Science and Engineering, Faculty of Mechanical, Maritime and Materials Engineering (3mE), Delft University of Technology, 2628 CD Delft, Netherlands; [orcid.org/0000-0003-4679-1752](https://orcid.org/0000-0003-4679-1752); Email: [p.dey@tudelft.nl](mailto:p.dey@tudelft.nl)

**Sampath Kumar Puttapati** – Department of Chemical Engineering, National Institute of Technology, Warangal, Telangana 506004, India; [orcid.org/0000-0002-7435-2215](https://orcid.org/0000-0002-7435-2215); Email: [pskr@nitw.ac.in](mailto:pskr@nitw.ac.in)

### Authors

**Anoop Kishore Vatti** – Department of Chemical Engineering, Manipal Institute of Technology (MIT), Manipal Academy

of Higher Education (MAHE), Manipal, Karnataka 576104, India; [orcid.org/0000-0003-3023-3684](https://orcid.org/0000-0003-3023-3684)

**Sriprasad Acharya** – Department of Chemical Engineering, Manipal Institute of Technology (MIT), Manipal Academy of Higher Education (MAHE), Manipal, Karnataka 576104, India

**Laxman Kumar Kunderapu** – Department of Chemical Engineering, Manipal Institute of Technology (MIT), Manipal Academy of Higher Education (MAHE), Manipal, Karnataka 576104, India

Complete contact information is available at:

<https://pubs.acs.org/10.1021/acs.energyfuels.2c02076>

## Notes

The authors declare no competing financial interest.

## ACKNOWLEDGMENTS

A.K.V. thank the Schrödinger Centre for Molecular Simulations, MAHE, Manipal, India, for their support. A.K.V. and S.A. would also like to thank Prof. Bharath Raj Guru for the optical microscopy facility.

## REFERENCES

- (1) *Asphaltenes: Fundamentals and Applications*; Sheu, E. Y., Mullins, O. C., Eds.; Springer: New York, 1995; DOI: [10.1007/978-1-4757-9293-5](https://doi.org/10.1007/978-1-4757-9293-5).
- (2) Saniere, A.; Hénaut, I.; Argillier, J. F. Pipeline Transportation of Heavy Oils, a Strategic, Economic and Technological Challenge. *Oil Gas Sci. Technol.* **2004**, *59*, 455–466.
- (3) Merdrignac, I.; Espinat, D. Physicochemical Characterization of Petroleum Fractions: The State of the Art. *Oil Gas Sci. Technol.* **2007**, *62*, 7–32.

- (4) Akbarzadeh, K.; Hammami, A.; Kharrat, A.; Zhang, D.; Allenson, S.; Creek, J.; Kabir, S.; Jamaluddin, A.; Marshall, A. G.; Rodgers, R. P.; Mullins, O. C.; Solbakken, T. Asphaltenes—Problematic but rich in potential. *Oilfield Rev.* **2007**, *19*, 22–43.
- (5) Alomair, O. A.; Almusallam, A. S. Heavy Crude Oil Viscosity Reduction and the Impact of Asphaltene Precipitation. *Energy Fuels* **2013**, *27*, 7267–7276.
- (6) Ilyin, S.; Arinina, M.; Polyakova, M.; Bondarenko, G.; Konstantinov, I.; Kulichikhin, V.; Malkin, A. Asphaltenes in heavy crude oil: Designation, precipitation, solutions, and effects on viscosity. *J. Pet. Sci. Eng.* **2016**, *147*, 211–217.
- (7) Rashid, Z.; Wilfred, C. D.; Gnanasundaram, N.; Arunagiri, A.; Murugesan, T. A comprehensive review on the recent advances on the petroleum asphaltene aggregation. *J. Pet. Sci. Eng.* **2019**, *176*, 249–268.
- (8) Spiecker, P.; Gawrys, K. L.; Kilpatrick, P. K. Aggregation and solubility behavior of asphaltenes and their subfractions. *J. Colloid Interface Sci.* **2003**, *267*, 178–193.
- (9) Yen, T. F. Asphaltenes. In *Structures and Dynamics of Asphaltenes*; Sheu, E. Y., Mullins, O. C., Eds.; Springer: Boston, MA, 1998; pp 1–20, DOI: 10.1007/978-1-4899-1615-0\_1.
- (10) Vatti, A. K.; Caratsch, A.; Sarkar, S.; Kandarapu, L. K.; Gadag, S.; Nayak, U. Y.; Dey, P. Asphaltene Aggregation in Aqueous Solution Using Different Water Models: A Classical Molecular Dynamics Study. *ACS Omega* **2020**, *5*, 16530–16536.
- (11) Sjöblom, J.; Aske, N.; Auflem, I. H.; Brandal, Ø.; Havre, T. E.; Sæther, Ø.; Westvik, A.; Johnsen, E. E.; Kallevik, H. Our current understanding of water-in-crude oil emulsions: Recent characterization techniques and high pressure performance. *Adv. Colloid Interface Sci.* **2003**, *100–102*, 399–473.
- (12) Pierre, C.; Barré, L.; Pina, A.; Moan, M. Composition and Heavy Oil Rheology. *Oil Gas Sci. Technol.* **2004**, *59*, 489–501.
- (13) Mitchell, D. L.; Speight, J. G. The solubility of asphaltenes in hydrocarbon solvents. *Fuel* **1973**, *52*, 149–152.
- (14) Li, X.; Sun, W.; Wu, G.; He, L.; Li, H.; Sui, H. Ionic Liquid Enhanced Solvent Extraction for Bitumen Recovery from Oil Sands. *Energy Fuels* **2011**, *25*, 5224–5231.
- (15) Zheng, C.; Brunner, M.; Li, H.; Zhang, D.; Atkin, R. Dissolution and suspension of asphaltenes with ionic liquids. *Fuel* **2019**, *238*, 129–138.
- (16) Sanati, A.; Malayeri, M.; Busse, O.; Weigand, J. Inhibition of asphaltene precipitation using hydrophobic deep eutectic solvents and ionic liquid. *J. Mol. Liq.* **2021**, *334*, 116100.
- (17) El-hoshoudy, A.; Ghanem, A.; Desouky, S. Imidazolium-based ionic liquids for asphaltene dispersion; experimental and computational studies. *J. Mol. Liq.* **2021**, *324*, 114698.
- (18) Ghanem, A.; Alharthy, R. D.; Desouky, S. M.; El-Nagar, R. A. Synthesis and Characterization of Imidazolium-Based Ionic Liquids and Evaluating Their Performance as Asphaltene Dispersants. *Materials* **2022**, *15*, 1600.
- (19) Lei, Z.; Chen, B.; Koo, Y.-M.; MacFarlane, D. R. Introduction: Ionic Liquids. *Chem. Rev.* **2017**, *117*, 6633–6635.
- (20) Painter, P.; Williams, P.; Mannebach, E. Recovery of Bitumen from Oil or Tar Sands Using Ionic Liquids. *Energy Fuels* **2010**, *24*, 1094–1098.
- (21) Berton, P.; Manouchehr, S.; Wong, K.; Ahmadi, Z.; Abdelfatah, E.; Rogers, R. D.; Bryant, S. L. Ionic Liquids-Based Bitumen Extraction: Enabling Recovery with Environmental Footprint Comparable to Conventional Oil. *ACS Sustainable Chem. Eng.* **2020**, *8*, 632–641.
- (22) Tian, Y.; McGill, W. B.; Whitcombe, T. W.; Li, J. Ionic Liquid-Enhanced Solvent Extraction for Oil Recovery from Oily Sludge. *Energy Fuels* **2019**, *33*, 3429–3438.
- (23) Boukherissa, M.; Mutelet, F.; Modarressi, A.; Dicko, A.; Dafri, D.; Rogalski, M. Ionic liquids as dispersants of petroleum asphaltenes. *Energy Fuels* **2009**, *23*, 2557–2564.
- (24) Ogunlaja, A. S.; Hosten, E.; Tshentu, Z. R. Dispersion of asphaltenes in petroleum with ionic liquids: Evaluation of molecular interactions in the binary mixture. *Ind. Eng. Chem. Res.* **2014**, *53*, 18390–18401.
- (25) Sakhthivel, S.; Velusamy, S.; Gardas, R. L.; Sangwai, J. S. Eco-efficient and green method for the enhanced dissolution of aromatic crude oil sludge using ionic liquids. *RSC Adv.* **2014**, *4*, 31007–31018.
- (26) Sakhthivel, S.; Velusamy, S.; Gardas, R. L.; Sangwai, J. S. Experimental investigation on the effect of aliphatic ionic liquids on the solubility of heavy crude oil using UV–visible, Fourier transform-infrared, and <sup>13</sup>C NMR spectroscopy. *Energy Fuels* **2014**, *28*, 6151–6162.
- (27) Subramanian, D.; Wu, K.; Firoozabadi, A. Ionic liquids as viscosity modifiers for heavy and extra-heavy crude oils. *Fuel* **2015**, *143*, 519–526.
- (28) Hernández-Bravo, R.; Miranda, A.; Martínez-Magadán, J.-M.; Domínguez, J. Experimental and Theoretical Study on Supramolecular Ionic Liquid (IL)–Asphaltene Complex Interactions and Their Effects on the Flow Properties of Heavy Crude Oils. *J. Phys. Chem. B* **2018**, *122*, 4325–4335.
- (29) Martínez-Mora, O.; Campa-Guevara, D.; Meza-Gordillo, R.; Sánchez, R.; Salas-Reyes, M.; Domínguez, J. M.; Matus, M. H.; Domínguez, Z. Imidazole-based ionic liquids as rheological modifiers of heavy crude oil: An experimental and theoretical study. *Aip Advances* **2021**, *11*, 035204.
- (30) Schermer, W. E. M.; Melein, P. M. J.; van den Berg, F. G. A. Simple Techniques for Evaluation of Crude Oil Compatibility. *Petroleum Science and Technology* **2004**, *22*, 1045–1054.
- (31) Li, X.; Guo, Y.; Boek, E. S.; Guo, X. Experimental Study on Kinetics of Asphaltene Aggregation in a Microcapillary. *Energy Fuels* **2017**, *31*, 9006–9015.
- (32) Soulgani, B. S.; Reisi, F.; Norouzi, F. Investigation into mechanisms and kinetics of asphaltene aggregation in toluene/n-hexane mixtures. *Petroleum Science* **2020**, *17*, 457–466.
- (33) Kandarapu, L. K.; Choudhury, S.; Acharya, S.; Vatti, A. K.; Pandiyan, S.; Gadag, S.; Nayak, U. Y.; Dey, P. Combined experimental and molecular dynamics investigation of 1D rod-like asphaltene aggregation in toluene-hexane mixture. *J. Mol. Liq.* **2021**, *339*, 116812.
- (34) Mullins, O. C.; Sabbah, H.; Eyssautier, J.; Pomerantz, A. E.; Barré, L.; Andrews, A. B.; Ruiz-Morales, Y.; Mostowfi, F.; McFarlane, R.; Goual, L.; Lepkowitz, R.; Cooper, T.; Orbulescu, J.; Leblanc, R. M.; Edwards, J.; Zare, R. N. Advances in Asphaltene Science and the Yen–Mullins Model. *Energy Fuels* **2012**, *26*, 3986–4003.
- (35) Groenzin, H.; Mullins, O. C. Asphaltene Molecular Size and Structure. *J. Phys. Chem. A* **1999**, *103*, 11237–11245.
- (36) Lu, C.; Wu, C.; Ghoreishi, D.; Chen, W.; Wang, L.; Damm, W.; Ross, G. A.; Dahlgren, M. K.; Russell, E.; Von Bargen, C. D.; Abel, R.; Friesner, R. A.; Harder, E. D. OPLS4: Improving Force Field Accuracy on Challenging Regimes of Chemical Space. *J. Chem. Theory Comput.* **2021**, *17*, 4291–4300.
- (37) Bowers, K. J.; Chow, E.; Xu, H.; Dror, R. O.; Eastwood, M. P.; Gregersen, B. A.; Klepeis, J. L.; Kolossvary, I.; Moraes, M. A.; Sacerdoti, F. D.; Salmon, J. K.; Shan, Y.; Shaw, D. E. Scalable Algorithms for Molecular Dynamics Simulations on Commodity Clusters. *Proceedings of the 2006 ACM/IEEE Conference on Supercomputing (SC '06)*; Tampa, FL, Nov 11–17, 2006; DOI: 10.1109/SC.2006.54.
- (38) Schrödinger Release 2021-1: *Desmond Molecular Dynamics System*; D. E. Shaw Research and Schrödinger, LLC: New York, 2021.
- (39) Ma, X.; Wang, W.; Sun, C.; Sun, J. Comprehensive evaluation of ionic liquid [Bmim][PF<sub>6</sub>] for absorbing toluene and acetone. *Environ. Pollut.* **2021**, *285*, 117675.
- (40) Milstein, J. N.; Meiners, J.-C. Worm-Like Chain (WLC) Model. In *Encyclopedia of Biophysics*; Roberts, G. C. K., Ed.; Springer: Berlin, Germany, 2013; pp 2757–2760, DOI: 10.1007/978-3-642-16712-6\_502.
- (41) Brinkers, S.; Dietrich, H. R. C.; de Groot, F. H.; Young, I. T.; Rieger, B. The persistence length of double stranded DNA determined using dark field tethered particle motion. *J. Chem. Phys.* **2009**, *130*, 215105.

(42) *Understanding Molecular Simulation*, 2nd ed.; Frenkel, D., Smit, B., Eds.; Academic Press: San Diego, CA, 2002; DOI: 10.1016/B978-0-12-267351-1.X5000-7.

## Recommended by ACS

### Ordering and Nonideality of Air–Ionic Liquid Interfaces in Surface Second Harmonic Generation

Renata Costa, Emmanuel Benichou, *et al.*

APRIL 23, 2020  
THE JOURNAL OF PHYSICAL CHEMISTRY B

READ 

### Structurally Related Scaling Behavior in Ionic Systems

S. Cheng, M. Paluch, *et al.*

JANUARY 30, 2020  
THE JOURNAL OF PHYSICAL CHEMISTRY B

READ 

### Long-Range Organization Study of Piperidinium-Based Ionic Liquids by Polarizable Molecular Dynamics Simulations

Sébastien Le Crom, Magali Duvail, *et al.*

APRIL 26, 2022  
THE JOURNAL OF PHYSICAL CHEMISTRY B

READ 

### The Influence of Anion Structure on the Ionic Liquids/Au (100) Interface by Molecular Dynamics Simulations

Yue Wang and Guocai Tian

NOVEMBER 19, 2021  
LANGMUIR

READ 

Get More Suggestions >